nature physics

ARTICLES

https://doi.org/10.1038/s41567-022-01555-6

Entropy-driven order in an array of nanomagnets

Hilal Saglam[1], Ayhan Duzgun[2], Aikaterini Kargioti[1], Nikhil Harle[3], Xiaoyu Zhang[1], Nicholas S. Bingham[1], Yuyang Lao[4], Ian Gilbert[4,10], Joseph Sklenar[4,5], Justin D. Watts[6,7], Justin Ramberger[6], Daniel Bromley[8], Rajesh V. Chopdekar[9], Liam O'Brien[8], Chris Leighton[6], Cristiano Nisoli[2] ✉ and Peter Schiffer[1,3,4] ✉

Long-range ordering is typically associated with a decrease in entropy. Yet, it can also be driven by increasing entropy in certain special cases. Here we demonstrate that artificial spin-ice arrays of single-domain nanomagnets can be designed to produce such entropy-driven order. We focus on the tetris artificial spin-ice structure, a highly frustrated array geometry with a zero-point Pauling entropy, which is formed by selectively creating regular vacancies on the canonical square ice lattice. We probe thermally active tetris artificial spin ice both experimentally and through simulations, measuring the magnetic moments of the individual nanomagnets. We find two-dimensional magnetic ordering in one subset of these moments, which we demonstrate to be induced by disorder (that is, increased entropy) in another subset of the moments. In contrast with other entropy-driven systems, the discrete degrees of freedom in tetris artificial spin ice are binary and are both designable and directly observable at the microscale, and the entropy of the system is precisely calculable in simulations. This example, in which the system's interactions and ground-state entropy are well defined, expands the experimental landscape for the study of entropy-driven ordering.

The somewhat paradoxical phenomenon of long-range ordering driven by maximizing entropy is observed in only a few systems in nature[1], such as vibrofluidized hard spheres, in which ordering maximizes the spheres' so-called free volume[2,3]. Often, ordering in one subset of degrees of freedom is driven by the possibility of increasing entropy in another subset, and thus of the total entropy. For instance, in the thin rod model of Onsager[4], rods order nematically to increase their translational entropy[5–8]. Entropy-driven ordering has been demonstrated primarily in out-of-equilibrium soft-matter systems such as colloids, hard-sphere suspensions and liquid crystals, where it has importance in self-assembly[9,10] for systems of biological and technological relevance[3,5,8,11–14]. Furthermore, entropy maximization is also implicated in the formation of high-entropy alloys of metallurgical importance[15].

While these effects have been studied in chemistry and in the physics of soft matter, a related yet different phenomenon in magnetic materials, so-called order by disorder[16,17], pertains instead to the interaction of spins arranged on a lattice in magnetic materials where collective excitations among magnetic moments select an ordered rather than disordered configuration in the ground state[18–23].

In this Article, we report entropy-driven ordering in an artificial spin ice, a structurally ordered nanomagnet array[24,25]. Specifically, we examine entropy-driven ordering in tetris artificial spin ice (referred to as 'tetris ice' for the remainder of the paper)[26,27]. We demonstrate a different paradigm for such ordering, quite distinct from what has been observed previously. Crucially, ordering in this system has strong similarities to the soft-matter systems described above, even though tetris ice is a structured nanomagnet array with no mechanical motion. Its degrees of freedom are, instead, the binary orientations of the nanoscale moments that are configured through thermalization.

Artificial spin ices can serve as models for a wide range of unusual physics unavailable in other systems because they can be lithographically designed at will. The ability to probe the magnetic degrees of freedom at the resolution of a single magnetic moment has provided the first realizations of celebrated vertex models[28] and also led to experimental demonstrations of a number of new models for collective behaviour[24,25,29]. Relevant to our study, the characteristic that the individual magnetic degrees of freedom are constrained to point in one of two directions for each moment sets tetris ice apart from the entropy-driven orderings referenced above.

The structure of tetris ice is obtained by selective removal of moments from the canonical square ice structure, as illustrated in Fig. 1a,b. This system belongs to a category of artificial spin ices that are 'vertex-frustrated'[26,29], that is, structured such that every lattice vertex cannot have its moments arranged in their local low-energy configuration. As a result, the system necessarily has multiple 'unhappy vertices' that are excited out of their local vertex ground states, as well as zero-point entropy associated with the degeneracy in allocating the unhappy vertices within the lattice.

We start our discussion of the collective states of tetris ice with a description of the energy and entropy of moment configurations at low energy. As indicated in Fig. 1b, the system's lowest-energy manifold is composed of two different one-dimensional subsystems of alternating stripes of moments, so-called backbones (BBs) and staircases (SCs)[26,27]. In the system's ground state, the SC moments contain unhappy vertices and are disordered. Moreover, the individual SC zero-temperature disorder, and thus its correlations, are well described by a disordered one-dimensional Ising phase[27].

[1]Department of Applied Physics, Yale University, New Haven, CT, USA. [2]Theoretical Division and Center for Nonlinear Studies, Los Alamos National Laboratory, Los Alamos, NM, USA. [3]Department of Physics, Yale University, New Haven, CT, USA. [4]Department of Physics, University of Illinois at Urbana-Champaign, Urbana, IL, USA. [5]Department of Physics and Astronomy, Wayne State University, Detroit, MI, USA. [6]Department of Chemical Engineering and Materials Science, University of Minnesota, Minneapolis, MN, USA. [7]School of Physics and Astronomy, University of Minnesota, Minneapolis, MN, USA. [8]Department of Physics, University of Liverpool, Liverpool, UK. [9]Advanced Light Source, Lawrence Berkeley National Laboratory, Berkeley, CA, USA. [10]Present address: Seagate Research Group, Seagate Technology, Shakopee, MN, USA. ✉e-mail: cristiano@lanl.gov; peter.schiffer@yale.edu

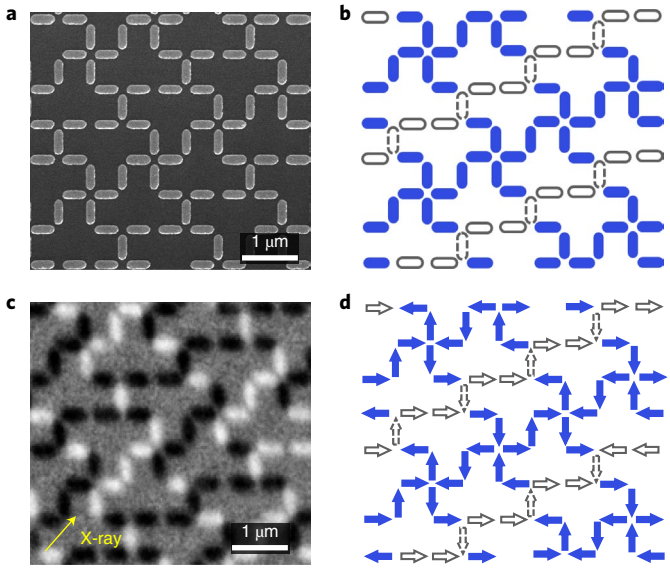

Fig. 1 | Tetris artificial spin ice. a, Scanning electron microscopy image of a tetris artificial spin ice (sample A). **b**, Schematic of the tetris ice structure, showing BB nanomagnet islands (blue) and SC islands (grey) with vertical (dashed borders) and horizontal moments (solid borders). The longitudinal direction is defined as the direction parallel to the stripes, approximately 26.5° from the horizontal, and the transverse direction as perpendicular to that. **c**, XMCD-PEEM image of the tetris ice lattice, showing the direction of the incident X-ray beam (yellow arrow). The islands that have a magnetization component along (opposite to) the X-ray direction yield black (white) contrast (sample A at $T = 120$ K). **d**, Magnetic moment configuration map corresponding to **c** with the same colour scheme as in **b**.

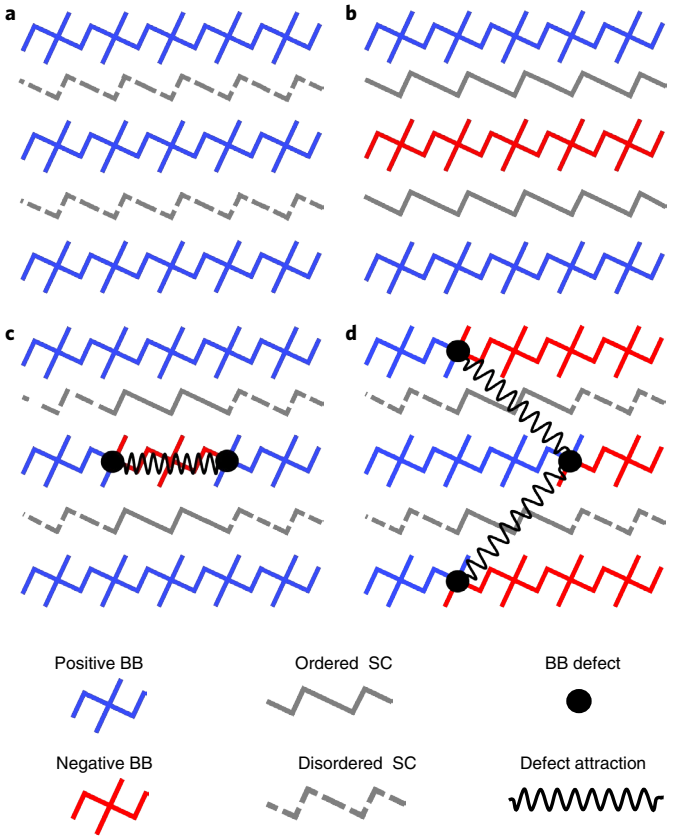

Fig. 2 | Entropic interactions in tetris ice. a, Schematic of a ground-state configuration that leads to maximal disorder in SCs due to the transverse ordering among the BBs, all having the same $\langle\Psi\rangle$. **b**, Schematic of a ground-state configuration where BBs alternate their order parameter $\langle\Psi\rangle$, leading to the SC moments being ordered. **c**, Schematic of BB defect attraction where two longitudinal defects attract each other due to the entropy cost of ordering portions of the adjacent SCs. **d**, Schematic of BB defect attraction across multiple BBs, where BB defects attract each other due to the entropy cost of ordering portions of the adjacent SCs, thus favouring two-dimensional domain walls that cross multiple BBs. Moment orientations that correspond to these schematics are shown in Supplementary Fig. 2.5.

In contrast, the BB moments do not contain any unhappy vertices and are ordered longitudinally, that is, along the length of the stripes. Within a nearest-neighbour coupling approximation, a given ground-state configuration of the array receives no energetic advantage from being transversely ordered, meaning that mutual order among the different BBs is neither favoured nor disfavoured energetically[26].

To characterize ordering among the BB moments, we use the staggered order parameter, $\langle\Psi\rangle = (-1)^{i+j} S_{ij}^{BB}$, where S_{ij}^{BB} denotes the polarization of the BB moments and i and j are the vertical and horizontal location indices of the moments in the underlying square ice lattice[28]. Note that Ψ here is simply the standard antiferromagnetic order parameter for the ordering of square ice: the average value $\langle\Psi\rangle = \pm 1$ corresponds to the two equivalent ordered ground states of that lattice. In other words, two ordered BBs have the same $\langle\Psi\rangle$ if their moments' orientations belong to the same ground state of the underlying square lattice.

Figure 2a schematically illustrates the case of neighbouring BBs in the ground state with the same $\langle\Psi\rangle$. It has been proven that, in this configuration, the ground state of the SC moments between the BBs is necessarily disordered[26]. An alternative ground state for the system has neighbouring BBs with values of $\langle\Psi\rangle$ alternating between +1 and −1 (Fig. 2b). In this other ground-state configuration, the SC moments between the BBs must be ordered[26]. These two alternative ground-state configurations have the same energy, but the disorder in the SCs of the former gives an entropic advantage for neighbouring BBs to have the same value of $\langle\Psi\rangle$. Thus, there is an entropic advantage for the entire two-dimensional system to have all BBs with either $\langle\Psi\rangle = 1$ or $\langle\Psi\rangle = -1$, implying two-dimensional order among the BB moments. In other words, the BBs order to the same $\langle\Psi\rangle$ to gain global entropy for the system, which comes from the entropy of the disordered SC moments. The system sacrifices the entropy that it would gain by having randomness in the value of $\langle\Psi\rangle$ among different BBs because that entropy scales subextensively (since $\langle\Psi\rangle$ is binary, the entropy of a BB-disordered configuration is proportional to the number of BBs in the system, which scales as the square root of the area of the array). In doing so, the system gains entropy from the SCs, which instead scales extensively, that is, with the system size (Supplementary Section 5).

Entropy maximization implies mutual transverse ordering among BBs, but it also explains the longitudinal ordering within a single BB. Consider a configuration of ordered BBs all with the same $\langle\Psi\rangle$ but in which one BB has a finite longitudinal domain of length L_d with opposite $\langle\Psi\rangle$ (Fig. 2c). The two defects induce two ordered regions on the adjacent SCs, above and below the domain, corresponding to an increase in the SC free energy of approximately $\Delta F = K + TL_d s_{SC}$, where K is the energy of the domain boundaries, T is the system temperature, and s_{SC} is the entropy per moment of the disordered SC (Supplementary Section 5). This entropic term in the free energy yields a constant attraction $\sim Ts_{SC}$ among the two defects, suppressing the growth of the bound domain. This purely entropic interaction is crucial to explain the individual longitudinal

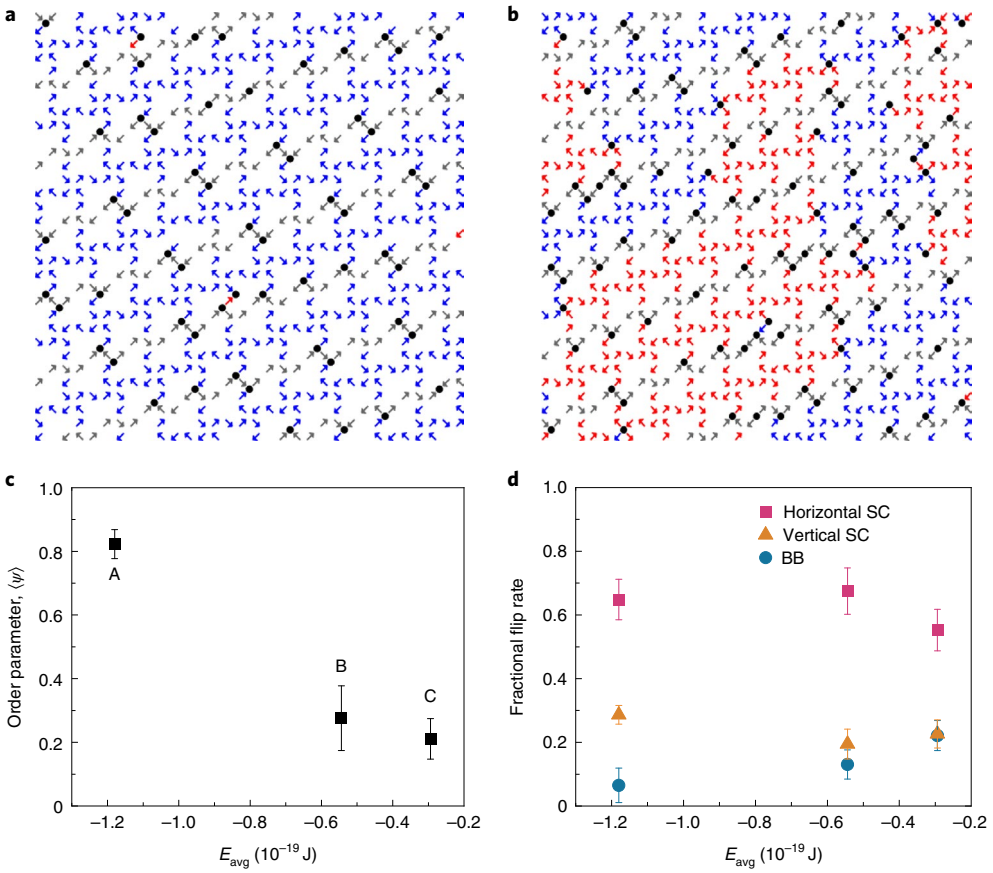

Fig. 3 | Two-dimensional ordering in tetris ice. a, Digitized XMCD-PEEM snapshot of tetris ice near the ground state, showing single-domain ordering of the BBs (sample A at $T = 120$ K). **b**, Digitized XMCD-PEEM snapshot of tetris ice above the ground state, showing BBs ordering in two-dimensional domains while the SCs remain disordered (sample B at $T = 190$ K). Black dots indicate unhappy vertices. The red and blue arrows indicate regimes of opposite antiferromagnetic order parameter. **c**, Staggered antiferromagnetic order parameter for the BB moments plotted as a function of increasing average vertex energy from sample A to C. **d**, Relative probability of flipping for BB, horizontal and vertical SC islands, that is, the fractional flip rate, showing that more than 80% of the kinetics is in the SCs. Error bars show the s.d. of the data collected at different temperatures.

ordering of the BBs since, as a one-dimensional system, a single BB would not be expected to order without this attractive interaction among defects. Using similar reasoning, one can show that defects on neighbouring BBs also interact entropically, favouring their alignment into two-dimensional domain walls (Fig. 2d).

We now turn to experimental studies of this system. We have experimentally investigated the entropy-driven ordering in tetris ice through X-ray magnetic circular dichroism photoemission electron microscopy (XMCD-PEEM) measurements on three samples of tetris ice composed of thin permalloy ($Ni_{80}Fe_{20}$) nanoislands. The thickness (~3 nm) was chosen so that the island moments were thermally active in the measurement temperature range, that is, thermal moment reversals occurred on the time scale of imaging. The samples (A, B and C) had different interaction strengths between neighbouring moments, associated with differences in the island size and spacing. Sample A (studied previously[27]) had the strongest interactions while sample C had the weakest interactions, based on micromagnetic calculations[30]. A representative scanning electron microscopy image is shown in Fig. 1a, and detailed descriptions of the samples and measurements are given in Methods and Supplementary Section 1).

The XMCD-PEEM technique allows full-field imaging of moment orientations in the lattice on time scales on the order of seconds. A typical XMCD-PEEM image is shown in Fig. 1c, and the corresponding map of moment directions is shown in Fig. 1d. In the temperature range studied for each sample (see Supplementary Section 2 for details), the system ranged from the moments fluctuating faster than the images could capture at the highest temperatures to the moments being effectively frozen at the lowest temperatures. We note that this technique has been demonstrated previously to effectively thermalize the moments in artificial spin ice[31] and has been used extensively under the assumption of thermalization[24,25]. For all of the samples, the temperature dependence of the average vertex statistics is quite small, suggesting that the system thermalized at room temperature, and relaxed upon cooling to a metastable moment configuration within which the moments fluctuated without further reducing the overall system energy. This suggests that further relaxation to the ground state is limited by the complex topology of the lattice[32,33], in combination with intrinsic structural disorder associated with limitations of the lithography.

Figure 3a,b shows schematics of the digitized moment configurations obtained from XMCD-PEEM measurements of two samples with different interaction strengths and therefore different proximity to the ground state. Figure 3a shows a moment configuration close to the ground state, demonstrating close to full two-dimensional ordering of the BBs, coexisting with disorder in the SCs. Note that the ordered configurations in the BBs correspond to those of the antiferromagnetic ground state of square ice from which the tetris ice structure is obtained, but the disordered moments on the SCs do not. This ordering is apparent in the series of so-called type I vertices[2] in the BBs that correlate both along the BBs and across them, leading to visible structure in the moment orientation, that is,

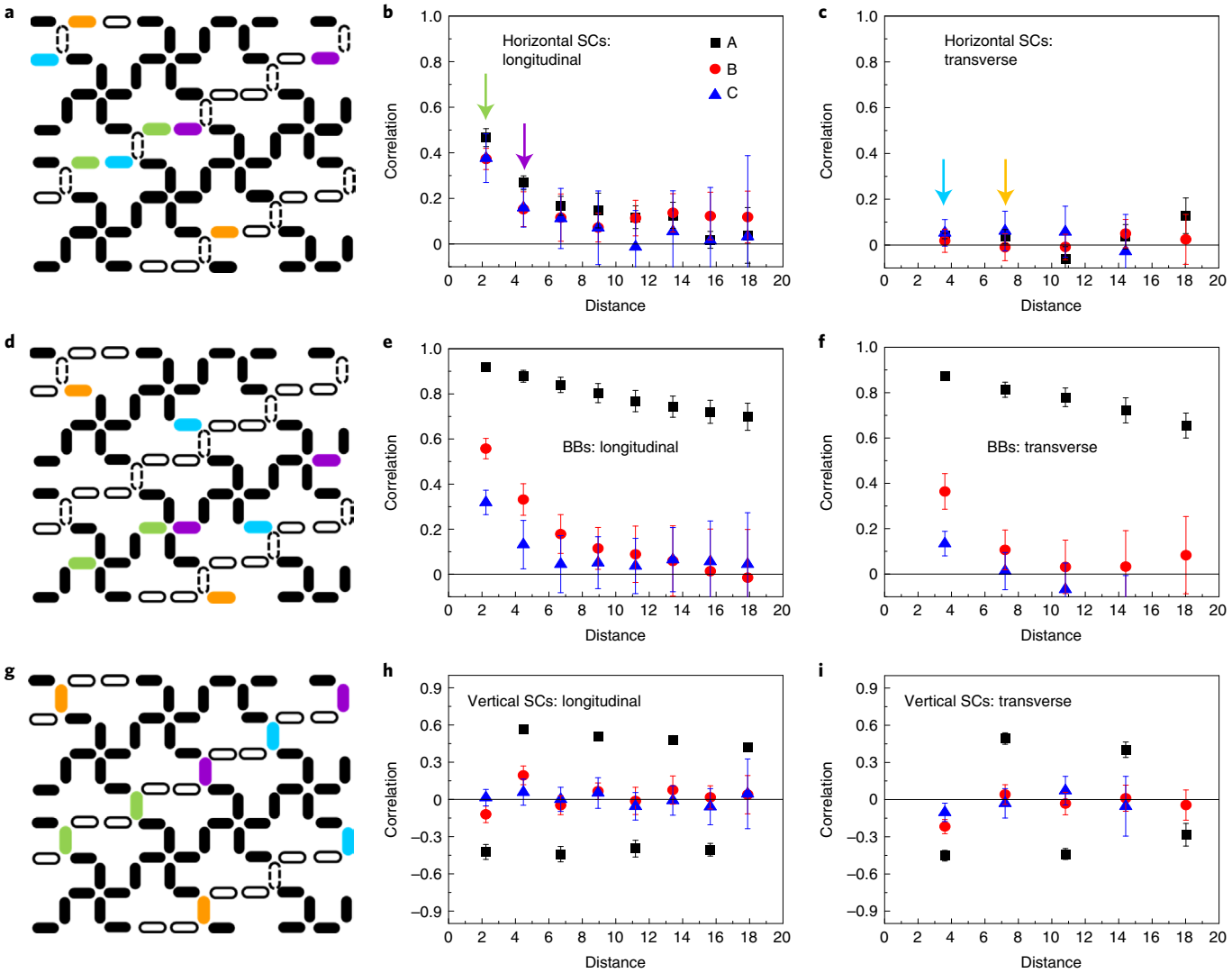

Fig. 4 | Longitudinal and transverse moment correlations. a, Schematic of the tetris ice structure highlighting the horizontal SC islands, showing the two horizontal SC islands that are each other's nearest neighbours in the longitudinal (green) and transverse direction (blue) as well as the next-nearest neighbours in the longitudinal (purple) and transverse direction (orange). We do not consider the pairs of horizontal moments that are within a particular stair of the SCs, since such pairs are highly correlated. **b**, The average moment correlations as a function of distance (in units of the lattice constant of the underlying square ice lattice structure) within horizontal SCs (longitudinal correlations) for the three samples studied. **c**, The average moment correlations as a function of distance across the horizontal SCs (transverse correlations) for the three samples studied. **d**–**f**, As in **a**–**c** but for the BB moments. **g**–**i**, As in **a**–**c** but for the vertical SC moments. Error bars represent the s.d. of the data collected at different temperatures.

the formation of near-complete loops of approximate head-to-tail flux closure in the moment orientations, broken only by disorder on the SCs. Such structure can also be seen to a lesser extent in Fig. 3b, which shows a moment configuration somewhat further from the ground state with domain walls in the BBs between regions of different $\langle\Psi\rangle$.

Figure 3c shows the resulting order parameter $\langle\Psi\rangle$ as a function of the average vertex energy for the different samples, noting that the different interaction strengths associated with the differences among the samples lead to different energies in the thermalized states. The average vertex energy, E_{avg}, is defined as $E_{\mathrm{avg}} = \sum \varepsilon_\alpha N_\alpha / N_{\mathrm{total}}$, where N_α is the number of observed vertices of type α, ε_α is the vertex energy and N_{total} is the total number of vertices. The vertex energies, ε_α, were calculated using micromagnetic simulations[30] for different vertices, lattice constants and island dimensions (see Supplementary Section 3 for details). The numbers of vertices, N_α, were extracted from the XMCD-PEEM data. Since the temperature dependence of the vertex statistics was weak, we show data averaged over the full temperature range in which we took data (see Supplementary Section 2 for details).

Because $\langle\Psi\rangle$ in Fig. 3c is measured over the entire image, its increasing value with stronger interaction energy corresponds to a transverse ordering of the moments in the BBs. Figure 3d shows the fractional flipping rate of different moments in the system as a function of the interaction energy (defined as the fraction of the moment flips between successive frames that are among the BB moments, vertical SC moments or horizontal SC moments). The results show that the kinetics are largely confined to the disordered SCs, especially for the interaction energies of largest magnitude.

We now analyse the longitudinal and transverse correlations to quantify the two-dimensional order across the system. If S_{ij}^{BB} and $S_{i'j'}^{\mathrm{BB}}$ are two BB moments, we define their transverse and longitudinal correlations as $C_{\mathrm{BB}} = S_{ij}^{\mathrm{BB}} S_{i'j'}^{\mathrm{BB}} (-1)^{i-i'+j-j'}$, where $C_{\mathrm{BB}} = +1$ if the moments have the same value of Ψ and $C_{\mathrm{BB}} = -1$ if the values of Ψ are

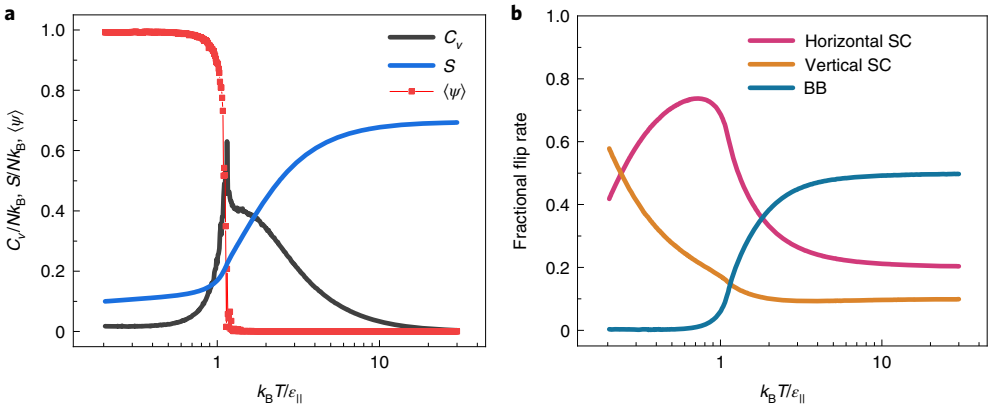

Fig. 5 | Two-dimensional ordering in tetris ice simulation. a, Specific heat (C_v), entropy (S) and order parameter $\langle\Psi\rangle$ for the BB moments versus temperature computed via Monte Carlo simulations (details provided in Supplementary Section 4). The specific heat shows a peak corresponding to the entropy-induced ordering transition of the BBs, while the entropy shows a residual value at zero temperature that is associated with the SCs. **b**, The temperature dependence of the moment fractional flip rates for different types of moments in the lattice.

opposite. For both horizontal and vertical SC moments, we instead define the usual ferromagnetic correlation, that is, $C_{SC} = S_{ij}^{SC} S_{i'j'}^{SC}$. Since we are primarily interested in longer-range correlations, we consider only those horizontal SC moments where the two adjacent moments in a step are aligned head to tail.

Figure 4 shows measured correlations among different moment pairs for the three samples, again averaged over all temperatures. The error bars here represent the s.d. of the data collected at different temperatures. Figure 4a defines the pairs of nearest- and next-nearest-neighbour moments, both longitudinally and transversely, through colour labels (similar definitions apply in Fig. 4d,g). Figure 4b plots longitudinal correlations of horizontal moments within the same SCs. Note that the distance dependence of the longitudinal moment correlations within the horizontal SCs does not change much among the samples, because those correlations are a property of the constrained disorder of the ground state. By contrast, there are considerable differences among the three samples in the longitudinal correlations within the BBs (Fig. 4e). They become increasingly more correlated with increasing interaction strength (from C to B to A), and the correlations evolve to an almost flat $\langle C_{BB}\rangle = 1$ value as a function of distance for sample A, as expected for the ground state.

We now consider correlations transverse to the BBs and SCs. Figure 4c shows no discernible transverse correlation among the horizontal moments of different SCs. In contrast, Fig. 4f reveals considerable transverse correlations among BB moments, with correlation values almost as large as in the longitudinal case (Fig. 4e). As in that case, they grow with increasing interaction strength, eventually approximating the flat $\langle C_{BB}\rangle = 1$ value that corresponds to two-dimensional long-range order. This can be seen clearly in real-space snapshots that reveal isotropic domains of various sizes (Supplementary Figs. 2.6–2.8). The contrasting complete lack of transverse order among the horizontal SC moments is a clear indication of the separation of the BBs and the SCs in terms of their entropy, with the entropy of the BBs minimized and the entropy of the SCs (and thus of the whole system) maximized. Note that, because the SCs separate the BBs, the impressive ordering of the BB moments is strong evidence for the entropically mediated interactions among the BBs. Our Monte Carlo simulations, discussed below, show that a near-neighbour model, with no interaction whatsoever among BBs, replicates these experimental findings (Supplementary Fig. 4.2).

Completing our discussion of Fig. 4, the correlations among the vertical moments in the SCs are shown in Fig. 4h,i. We observe that the correlation among the vertical moments is almost flat in magnitude (but alternating in sign), as if they were ordered, but the value of the correlation is $|\langle C_{SC}\rangle| \sim 0.5$ for sample A and smaller for samples B and C. These moments thus possess features of both long-range order (correlation almost constant in space) as well as disorder, in the sense that $|\langle C_{SC}\rangle|$ never approaches unity, even for near neighbours. As shown in Supplementary Section 6, correlations among vertical SC moments are dictated both by horizontal SC moments, which are disordered, and also by the BB moments surrounding the SCs, which are ordered. A value of $|\langle C_{SC}\rangle| = 0.5$ is expected in the system ground state. This sort of half-ordering of the vertical moments is highly unusual in magnetic systems. It is neither short-range ordering, which should approach $|\langle C_{SC}\rangle| \sim 1$ at short distances along a given lattice direction and fall sharply with increasing separation, nor a disordered state, as the absolute value of the correlation persists at nearly the same value with distance. Rather, this represents a consequence of the peculiar frustration in tetris ice.

We now discuss simulations of this system, which enhance our understanding of the experimental results. The attribution of transverse ordering to entropic effects assumes that the ordering does not arise from long-range interactions among the moments. To confirm that long-range interactions are not needed to explain the ordering, we performed Metropolis Monte Carlo simulations within a vertex model that considers only interactions among moments that share a common vertex. This excludes interactions amongst the moments belonging to different BBs and SCs and thus provides an important corroboration of the entropy-induced mechanism of the BB ordering. Significantly, because the Monte Carlo simulation produces a collective state that mirrors what we see in experiment, it provides a separate validation that our experimental system was well thermalized (details of the Monte Carlo results are given in Supplementary Section 4).

Figure 5a shows the entropy, the specific heat and the order parameter $\langle\Psi\rangle$ from our simulations, as functions of temperature. We note the sharp peak in the specific heat, associated with ordering of the BBs. The transition temperature corresponds to the energy scale of vertex interaction energies, which indicates that longer-range interactions are not driving the transition, a conclusion that is also suggested by the disorder on the SC moments. The observation of an ordering transition among the BB moments, a disordered state among the SC moments and a residual entropy for the system, which must be associated with that disorder, shows the clear separation of the entropy among the two subsets of moments.

Because the BB moments are ordered, this simulation also provides a quantification of the entropy associated with the SC disorder.

Figure 5b plots the corresponding temperature dependence of the moment fractional flip rates, showing how the dynamics of the system below the ordering temperature is confined to the SC moments. Note that the fractional flip rates for both vertical and horizontal SCs are non-zero at the lowest temperatures and the vertical SC fractional flip rate rises continuously as the temperature decreases, suggesting that those are the most active moments. This again points to the distinct behaviour of the BB and SC moments within the tetris ice structure, despite being strongly correlated.

We also use our Monte Carlo simulations to demonstrate entropy-based ordering in a situation that cannot be easily reproduced experimentally. Specifically, we initiate the system in a ground-state configuration corresponding to an order parameter of zero, that is, $\langle\Psi\rangle=\pm1$ on alternating BBs (Supplementary Fig. 4.3a). We then allow the system to evolve at a temperature of only $\sim0.3T_C$, where T_C is the ordering temperature for the BBs. Our simulations show that the system spontaneously evolves through thermal fluctuations into a BB-ordered state corresponding to uniform $\langle\Psi\rangle=1$ (Supplementary Fig. 4.3b). This further supports the robust nature of the observed entropically driven ordering among BB moments since it can be obtained through multiple thermodynamic paths, not just through cooling from high temperature.

We now compare our entropy-driven ordering with similar phenomena in other systems. Our observed ordering in the tetris ice system is substantially different from the so-called order by disorder found in some other magnetic systems[16–23]. In those cases, fluctuations can lift the degeneracy of the ground state by selecting ordered states of lower energy excitation. In our case, however, the very ground-state manifold at zero temperature 'favours' order, because this order maximizes the residual entropy that results from frustration. Indeed, configurations with ordered BBs numerically dominate the ground-state manifold in the large size limit, as demonstrated in Supplementary Section 5.

The tetris ice system is therefore conceptually closer in nature to the entropy-based ordering seen in structurally disordered materials, where some degrees of freedom become ordered to enable more entropy in other degrees of freedom. A paradigmatic example is the nematic ordering of rod-shaped objects in the seminal Onsager model[1,4]. The tetris ice system similarly has two distinct and competing entropies, that of the SC moments and that of the BB moments. The latter is reduced to maximize the former, a mechanism which maximizes the total entropy, analogous to the Onsager model. An important difference, however, is that the tetris ice system is well structured around a specific geometry, with discrete degrees of freedom that are accessible experimentally. While the two entropies correspond in the Onsager model to different coordinates of the same rods, in tetris ice they refer to different positions in a lattice. The two cases are mathematically similar in that the entropy of a subset of degrees of freedom is reduced to maximize the total entropy, but the nature of the degrees of freedom are strikingly different, mechanical and continuous in the former, binary in the latter, distinctly separating the two cases.

Many groups have now established that frustration in a magnetic system can result in a residual entropy, with the spin-ice pyrochlore materials providing an excellent example[34]. Our findings go considerably further, demonstrating that such residual entropy can drive robust ordering in a frustrated magnetic system. This suggests that a range of other artificial spin-ice geometries could be designed to tune the balance between energetic and entropic effects in ordering of moments, a possibility that would be quite difficult to realize in other physical systems.

The observation of entropy-driven magnetic ordering in the tetris ice system also adds a new category to the types of systems that display entropy-driven ordering. While our experiments are driven purely through thermal effects, the addition of quantum fluctuations[35] will likely drive yet more exotic phenomena associated with entropic considerations. Future studies will be able to probe additional bespoke artificial spin ice structures with ground state entropy that favours other types of ordering phenomena. More generally, our results show how non-trivial forms of frustration can be used to generate unusual, even apparently paradoxical phenomena that are broadly related to other physical phenomena in disparate systems[1], and to do so in ways that enable more detailed studies of the microscopic driving behaviour.

Online content

Any methods, additional references, Nature Research reporting summaries, source data, extended data, supplementary information, acknowledgements, peer review information; details of author contributions and competing interests; and statements of data and code availability are available at https://doi.org/10.1038/s41567-022-01555-6.

Received: 19 May 2021; Accepted: 18 February 2022;
Published online: 07 April 2022

References

1. Frenkel, D. Order through entropy. *Nat. Mater.* **14**, 9–12 (2015).
2. Percus, J. K. (ed.) *The Many-Body Problem* (Interscience, 1963).
3. Lin, K.-H. et al. Entropically driven colloidal crystallization on patterned surfaces. *Phys. Rev. Lett.* **85**, 1770–1773 (2000).
4. Onsager, L. The effects of shape on the interaction of colloidal particles. *Ann. N. Y. Acad. Sci.* **51**, 627–659 (1949).
5. Fraden, S., Maret, G., Caspar, D. L. D. & Meyer, R. B. Isotropic-nematic phase transition and angular correlations in isotropic suspensions of tobacco mosaic virus. *Phys. Rev. Lett.* **63**, 2068–2071 (1989).
6. van der Beek, D. & Lekkerkerker, H. N. W. Nematic ordering vs. gelation in suspensions of charged platelets. *Europhys. Lett.* **61**, 702–707 (2003).
7. Dussi, S. & Dijkstra, M. Entropy-driven formation of chiral nematic phases by computer simulations. *Nat. Commun.* **7**, 11175 (2016).
8. Kil, K. H., Yethiraj, A. & Kim, J. S. Nematic ordering of hard rods under strong confinement in a dense array of nanoposts. *Phys. Rev. E* **101**, 032705 (2020).
9. Filion, L. et al. Self-assembly of a colloidal interstitial solid with tunable sublattice doping. *Phys. Rev. Lett.* **107**, 168302 (2011).
10. Sciortino, F. Entropy in self-assembly. *Riv. Nuovo Cim.* **42**, 511–548 (2019).
11. Pusey, P. N. & van Megen, W. Phase behaviour of concentrated suspensions of nearly hard colloidal spheres. *Nature* **320**, 340–342 (1986).
12. Barry, E. & Dogic, Z. Entropy driven self-assembly of nonamphiphilic colloidal membranes. *Proc. Natl Acad. Sci. USA* **107**, 10348–10353 (2010).
13. Damasceno, P. F., Engel, M. & Glotzer, S. C. Predictive self-assembly of polyhedra into complex structures. *Science* **337**, 453–457 (2012).
14. Zhu, G., Huang, Z., Xu, Z. & Yan, L.-T. Tailoring interfacial nanoparticle organization through entropy. *Acc. Chem. Res.* **51**, 900–909 (2018).
15. Zhang, Y. et al. Microstructures and properties of high-entropy alloys. *Prog. Mater. Sci.* **61**, 1–93 (2014).
16. Villain, J., Bidaux, R., Carton, J.-P. & Conte, R. Order as an effect of disorder. *J. Phys.* **41**, 1263–1272 (1980).
17. Henley, C. L. Ordering due to disorder in a frustrated vector antiferromagnet. *Phys. Rev. Lett.* **62**, 2056–2059 (1989).
18. Zhitomirsky, M. E., Gvozdikova, M. V., Holdsworth, P. C. W. & Moessner, R. Quantum order by disorder and accidental soft mode in $Er_2Ti_2O_7$. *Phys. Rev. Lett.* **109**, 077204 (2012).
19. Plat, X., Fuji, Y., Capponi, S. & Pujol, P. Selection of factorizable ground state in a frustrated spin tube: order by disorder and hidden ferromagnetism. *Phys. Rev. B* **91**, 064411 (2015).
20. Guruciaga, P. C. et al. Field-tuned order by disorder in frustrated Ising magnets with antiferromagnetic interactions. *Phys. Rev. Lett.* **117**, 167203 (2016).
21. Ross, K. A., Qiu, Y., Copley, J. R. D., Dabkowska, H. A. & Gaulin, B. D. Order by disorder spin wave gap in the XY pyrochlore magnet $Er_2Ti_2O_7$. *Phys. Rev. Lett.* **112**, 057201 (2014).
22. Green, A. G., Conduit, G. & Krüger, F. Quantum order-by-disorder in strongly correlated metals. Annu. *Rev. Condens. Matter Phys.* **9**, 59–77 (2018).
23. Okuma, R. et al. Fermionic order by disorder in a van der Waals antiferromagnet. *Sci. Rep.* **10**, 15311 (2020).
24. Schiffer, P. & Nisoli, C. Artificial spin ice: paths forward. *Appl. Phys. Lett.* **118**, 110501 (2021).
25. Skjærvø, S. H., Marrows, C. H., Stamps, R. L. & Heyderman, L. J. Advances in artificial spin ice. *Nat. Rev. Phys.* **2**, 13–28 (2020).

26. Morrison, M. J., Nelson, T. R. & Nisoli, C. Unhappy vertices in artificial spin ice: new degeneracies from vertex frustration. *N. J. Phys.* **15**, 045009 (2013).
27. Gilbert, I. et al. Emergent reduced dimensionality by vertex frustration in artificial spin ice. *Nat. Phys.* **12**, 162–165 (2016).
28. Baxter, R. J. Spontaneous staggered polarization of the F-model. *J. Stat. Phys.* **9**, 145–182 (1973).
29. Nisoli, C., Kapaklis, V. & Schiffer, P. Deliberate exotic magnetism via frustration and topology. *Nat. Phys.* **13**, 200–203 (2017).
30. Vansteenkiste, A. et al. The design and verification of MuMax3. *AIP Adv.* **4**, 107133 (2014).
31. Farhan, A. et al. Direct observation of thermal relaxation in artificial spin ice. *Phys. Rev. Lett.* **111**, 057204 (2013).
32. Lao, Y. et al. Classical topological order in the kinetics of artificial spin ice. *Nat. Phys.* **14**, 723–727 (2018).
33. Zhang, X. et al. String phase in an artificial spin ice. *Nat. Commun.* **12**, 6514 (2021).
34. Ramirez, A. P., Hayashi, A., Cava, R. J., Siddharthan, R. & Shastry, B. S. Zero-point entropy in 'spin ice'. *Nature* **399**, 333–335 (1999).
35. King, A. D., Nisoli, C., Dahl, E. D., Poulin-Lamarre, G. & Lopez-Bezanilla, A. Qubit spin ice. *Science* **373**, 576–580 (2021).

Methods

Arrays of tetris artificial spin ice with various lateral dimensions and thicknesses were fabricated on silicon substrates with native oxide using electron beam lithography and lift-off as described in previous work[27,32,33]. The bilayer e-beam resist was spin-coated onto the substrate and exposed to the electron beam to write the desired structures. After development, permalloy ($Ni_{80}Fe_{20}$) films with varying thicknesses (2.5–3.5 nm) were deposited by ultra-high-vacuum electron beam evaporation at a rate of 0.5 Å s^{-1}. The base pressure of the system was 10^{-11} to 10^{-10} torr with a deposition pressure of 10^{-10} to 10^{-9} torr. Subsequently, a 2 nm capping layer of Al was deposited to prevent oxidation of the permalloy. The lattice constants and island sizes were measured using scanning electron microscopy and determined to be 602, 606 and 806 nm and 157×433, 157×433 and 178×483 nm^2 for sample A, B and C, respectively. Further details of the samples can be found in Supplementary Table 1.1. We performed XMCD-PEEM experiments on our tetris ice arrays at the PEEM-3 station at beamline 11.0.1.1 of the Advanced Light Source at Lawrence Berkley National Laboratory. Magnetic imaging was carried out at the Fe L3 edge. We conducted two XMCD-PEEM runs using different X-ray polarization sequences, exposure times and temperature ranges. The details of the XMCD-PEEM measurements can be found in Supplementary Table 2.1.

Data availability

Underlying data are available at https://datadryad.org/stash/share/-sT0veB190OcBSNk3G_ZW1qMa1yjbu7zjZhs-galmV0.

Acknowledgements

We thank I.-A. Chioar for fruitful discussions and A. Scholl for assistance with the early XMCD-PEEM measurements. Work at Yale University and the University of Illinois at Urbana-Champaign was funded by the US Department of Energy (DOE), Office of Basic Energy Sciences, Materials Sciences and Engineering Division under grant nos. DE-SC0010778 and DE-SC0020162 to H.S., A.K., N.H., X.Z., N.S.B., Y.L., I.G., J.S. and P.S. This research used resources of the Advanced Light Source, a DOE Office of Science User Facility under contract no. DE-AC02-05CH11231 to R.V.C. Work at the University of Minnesota was supported by NSF through grant nos. DMR-1807124 and DMR-2103711 to J.R., J.D.W. and C.L. Work at the University of Liverpool was supported by the UK Royal Society through grant no. RGS\R2\180208 to D.B. and L.O. Work at Los Alamos National Laboratory was carried out under the auspices of the US DOE through LANL, operated by Triad National Security, LLC under contract no. 892333218NCA000001 and financed by DOE LDRD (A.D. and C.N.).

Author contributions

J.R. and J.D.W. performed film depositions under the guidance of C.L., and D.B. prepared other samples under the guidance of L.O., with H.S., X.Z., I.G., Y.L., J.S. and N.S.B. overseeing the lithography. H.S., X.Z., I.G., Y.L., J.S., N.S.B. and R.V.C. performed the XMCD-PEEM characterization of the thermally active samples, and H.S., A.K. and N.H. analysed the data. H.S. performed micromagnetic calculations. A.D. performed Monte Carlo simulations, under the guidance of C.N. C.N. and P.S. supervised the entire project. All authors contributed to the discussion of results and to the finalization of the manuscript.

Competing interests

The authors declare no competing interests.

Additional information

Supplementary information The online version contains supplementary material available at https://doi.org/10.1038/s41567-022-01555-6.

Correspondence and requests for materials should be addressed to Cristiano Nisoli or Peter Schiffer.

Peer review information *Nature Physics* thanks Erik Folven, Alan Farhan and the other, anonymous, reviewer(s) for their contribution to the peer review of this work.